CHAPTER

16 Neuronal network architecture and temporal lobe epilepsy: A connectome-based and machine learning study

B.C. Munsell[1], G. Wu[2], S. Keller[3], J. Fridriksson[4], B. Weber[5], M. Styner[2], D. Shen[2], L. Bonilha[6]

College of Charleston, Charleston, SC, United States[1] University of North Carolina at Chapel Hill, Chapel Hill, NC, United States[2] University of Liverpool, Liverpool, United Kingdom[3] University of South Carolina, Columbia, SC, United States[4] University of Bonn, Bonn, Germany[5] Medical University of South Carolina, Charleston, SC, United States[6]

CHAPTER OUTLINE

Machine Learning and Medical Imaging. http://dx.doi.org/10.1016/B978-0-12-804076-8.00016-5
© 2016 Elsevier Inc. All rights reserved.

16.1 INTRODUCTION

Improvements in computational neuroimaging analyses now permit the assessment of whole brain maps of structural connectivity (Bartzokis, 2004; Sporns, 2011, 2013). By combining segmented gray matter tissue data from T1 weighted magnetic resonance imaging (MRI) with white matter fiber tractography from diffusion tensor imaging (DTI) MRI, it is possible to chart the organization of white matter connectivity across the entire brain, that is, the structural brain connectome (Sporns et al., 2005; Hagmann et al., 2008; Sporns, 2013). The brain connectome provides an unprecedented degree of information about the organization of neuronal network architecture, both at a regional level, as well as regarding the entire brain network. For this reason, the brain connectome has recently become instrumental in the investigation of neuronal systems organization and its relationship with health and disease, notably in the context of neurological conditions such as epilepsy (Bonilha, 2013, 2015; Besson, 2014; DeSalvo, 2014), schizophrenia (Rubinov and Bullmore, 2013; Crossley, 2014), and dementia (Xie and He, 2011; Daianu, 2013).

Epilepsy is a neurological disorder directly associated with pathological changes in brain network organization. Even though most forms of epilepsy are believed to arise from epileptogenic activity emerging from localized brain areas, there is a growing body of evidence suggesting that focal seizures are in reality the result of hyperexcitation of localized networks, rather than isolated cortical regions (Spencer, 2002; Richardson, 2012). Focal epilepsy is considered to be a disease of neuronal networks, where the aberrant structural and functional organization of neuronal systems leads to unabated neuronal hyper-excitability and seizures (Richardson, 2012). Even though histopathological changes were originally considered to be restricted to isolated brain regions, that is, hippocampal sclerosis in individuals with temporal lobe epilepsy (TLE) (Babb and Brown, 1987), there is a large and growing body of evidence from neuroimaging to suggest that more subtle abnormalities are pervasively distributed across multiple brain regions. In the case of TLE, regions that are functionally or structurally associated with the hippocampus demonstrate gray matter cell loss, white matter deafferentation, and pathological network architecture reorganization (Bernasconi, 2003, 2004; Bonilha, 2003, 2004; Bernhardt, 2008; Focke, 2008; Keller and Roberts, 2008). For this reason, epilepsy is now considered to be a condition that emanates from abnormal neuronal systems rather than isolated brain regions. Indeed, the concept of epilepsy as a neuronal network disorder features prominently in the newest epilepsy and seizures classification from the International League against epilepsy (Berg, 2010).

The clinical relevance of pervasive network abnormalities regarding seizure control is not yet completely understood. It stands to reason that more abnormally distributed networks may lead to different clinical endophenotypes regarding seizure control (Bonilha, 2012). Even though the advent of connectome-based research is still relatively recent, preliminary studies have not only demonstrated a consistent pattern of intra- and extratemporal connectivity abnormalities, but also individualized patterns of network abnormalities that may be directly associated with prognosis (Bonilha, 2015). Even though these are initial findings, they are a promising

indication of the pathological significance of connectome-based abnormalities in epilepsy.

Here, two different clinical studies are performed that apply machine learning techniques to create computational models capable of identifying abnormal network connections in structural brain connectomes reconstructed using white matter fiber tracts from DTI data. The aim and goal of each study is provided below, and the specific details are provided in Sections 16.2 and 16.3.

16.1.1 TREATMENT OUTCOME PREDICTION OF PATIENTS WITH TLE

The objective of this study is to evaluate machine learning algorithms aimed at predicting surgical treatment outcomes in groups of patients with TLE using only the structural brain connectome. A two-stage connectome-based prediction framework was developed that gradually selects a small number of abnormal network connections that contribute to the surgical treatment outcome, and in each stage a linear kernel operation is used to further improve the accuracy of the learned classifier. Using a 10-fold cross-validation strategy, the connectome-based prediction framework is able to separate patients with TLE from healthy controls with 80% accuracy, and is able to correctly predict the surgical treatment outcome of patients with TLE with 70% accuracy. Compared to existing state-of-the-art methods that use voxel-based morphometry data, the proposed connectome-based prediction framework is a suitable alternative with comparable prediction performance. Our results additionally show that machine learning algorithms that exclusively use structural connectome data can predict treatment outcomes in epilepsy with similar accuracy compared with "expert-based" clinical decision.

16.1.2 NAMING IMPAIRMENT PERFORMANCE OF PATIENTS WITH TLE

The objective of this study to evaluate the neuronal networks that support naming in TLE by using a machine learning algorithm intended to predict naming performance in subjects with medication refractory TLE using only the structural brain connectome reconstructed from DTI. A connectome-based prediction framework was developed using network properties from anatomically defined brain regions across the entire brain, which were used in a multitask machine learning algorithm followed by support vector regression. Nodal eigenvector centrality, a measure of regional network integration, predicted approximately 60% of the variance in naming. The nodes with the highest regression weight were bilaterally distributed among perilimbic subnetworks involving mainly the medial and lateral temporal lobe regions. In the context of emerging evidence regarding the role of large structural networks that support language processing, our results suggest intact naming relies on the integration of subnetworks, as opposed to being dependent on isolated brain areas. In the case of TLE, these subnetworks may be disproportionately indicative naming processes that are dependent on semantic integration from memory and lexical retrieval, as opposed to multimodal perception or motor speech production.

16.2 TREATMENT OUTCOME PREDICTION OF PATIENTS WITH TLE

16.2.1 PARTICIPANTS

A cohort of 70 patients with refractory TLE with hippocampal sclerosis or with medical refractory lesional TLE and a cohort of 48 healthy controls (HCs) were included in this study. TLE was diagnosed according to the criteria defined by the International League Against Epilepsy (ILAE, 1989), including a comprehensive neurological evaluation, ictal electroencephalography (EEG) recordings, diagnostic MRI, and, when appropriate, nuclear medicine studies. All TLE cases exhibited unilateral temporal lobe seizure onset during ictal EEG monitoring, and had routine diagnostic MRI revealing unilateral hippocampal atrophy. All patients with TLE underwent anterior temporal lobectomy or amygdalohippocampectomy. The surgical outcome was assessed based on the Engel Surgical Outcome scale (Engel, 2003) defined at least one year after surgery. In general, patients with TLE were classified into two groups: (1) free of disabling of seizures (ie, seizure-free), equivalent to Engel Class I (including Class 1b patients with auras only); and (2) not seizure-free, equivalent to Engel Classes II, III, or IV.

16.2.2 PRESURGICAL IMAGE ACQUISITION AND PROCESSING

The same imaging protocol was applied to all study participants (patients and controls). Images were acquired on a Siemens 3T Verio MRI scanner and the imaging protocol yielded a high-resolution T1-weighted image, with an isotropic voxel size of 1 mm. Diffusion-weighted images were obtained using two diffusion weightings along either 30 or 60 diffusion-encoding directions. DICOM images were converted to NIfTI format using the MRIcron software toolbox.[1] The FMRIB software library diffusion toolkit[2] (FDT) was used for preprocessing diffusion-weighted images and also for diffusion tensor estimation (Heiervang, 2006; Behrens, 2007). The images underwent eddy current correction through affine transformation of each DWI to the base $b = 0$, T2-weighted image.

16.2.3 PRESURGICAL CONNECTOME RECONSTRUCTION

Probabilistic tractography was used to define the number of white matter streamlines connecting each pair of cortical regions according to the Lausanne anatomical atlas that defines 82 regions of interest (ROIs). This step was iteratively performed until the connectivity between all possible pairs of cortical regions was determined. Structural connectivity was obtained by applying FDT's probabilistic method for fiber tracking (Behrens, 2003, 2007; Ciccarelli, 2006) and was performed on diffusion data after

[1] http://www.mccauslandcenter.sc.edu/mricro/mricron/dcm2nii.html
[2] http://www.fmrib.ox.ac.uk/fsl

voxel-wise calculation of the diffusion tensor. In general, probabilistic tractography was chosen because it is theoretically capable of accommodating intravoxel fiber crossings (Behrens, 2007; Nucifora, 2007). Cortical seed regions for tractography were obtained from an automatic segmentation process on the T1-weighted images that subdivided the human cerebral cortex into sulco-gyral-based cortical and subcortical ROIs defined in the anatomical atlas. All processed images were visually inspected to ensure the cortical segmentation quality. The ROIs were then transformed into each subject's DTI space using an affine transformation obtained with FSL's FLIRT.

For each subject, a comprehensive presurgical neural connectivity map or connectome is calculated, where the connectivity is measured by the number of probabilistic white matter fiber tract streamlines arriving at ROI j when ROI i was seeded, averaged with the number of probabilistic white matter fiber tract streamlines arriving at ROI i when ROI j was seeded. The step is iteratively repeated to ensure all 82 cortical ROIs are treated as seed regions. Once all iterations are completed, a symmetric 82×82 density connectivity map D is constructed, where D_{ij} corresponds to the weighted network between ROIs i and j. Since the number of streamlines between two different ROIs is averaged, D is symmetric with respect to the main diagonal. Three different example connectomes using the described reconstruction procedure are shown in Fig. 16.1. In particular, three examples are shown: (1) normal control, (2) patient with TLE that is seizure-free after surgery is performed, and (3) patient with TLE who is not seizure-free (ie, continues to experience seizures) after surgery.

16.2.4 CONNECTOME PREDICTION FRAMEWORK

The block diagram shown in Fig. 16.2 illustrates the basic design and operation of the proposed connectome-based prediction framework that defines a *Stage-1* prediction pipeline that is able to separate patients with TLE from normal controls, and a *Stage-2* prediction pipeline that is able to predict the surgical treatment outcome of patients with TLE. It is important to point out that the Stage-2 prediction pipeline is dependent on the Stage-1 prediction pipeline. That is, the output of the Stage-1 connectome feature selection component is the input to the Stage-2 connectome feature selection component. Furthermore, each prediction pipeline defines three trained components, that is, connectome feature selection, linear kernel operation, and linear SVM classifier, which are sequentially applied one after the other. The rationale behind the two-stage design is directly related to the number of network connections (ie, features) defined in the connectome. Specifically, using only one stage to identify a small subset of features (less than a hundred) from thousands that contribute to the surgical treatment outcome is a very challenging feature selection problem for any machine learning algorithm. Instead, the proposed two-stage design takes a more controlled approach by gradually reducing a high-dimension connectome feature space to a lower-dimension one, thus making the problem more tractable.

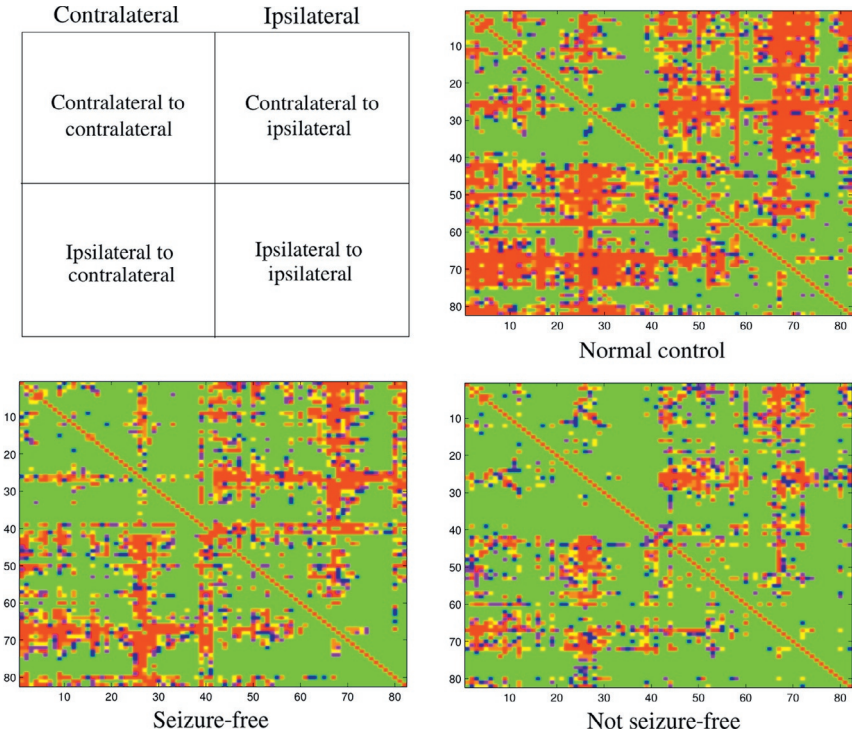

FIG. 16.1

Example connectomes are shown for a healthy control, a seizure-free patient, and a nonseizure-free patient. The brain structures are numbered from 1 to 82 in accordance with the chosen anatomical atlas. In particular, regions 1–42 represent the hemisphere contralateral to seizure onset, and 43–82 represent the hemisphere ipsilateral to seizure onset. Within each hemisphere, the regions are grouped as follows: frontal lobe, temporal lobe, basal nuclei, parietal lobe, and occipital lobe.

16.2.4.1 Connectome feature selection component

Assume an $n \times m$ training data matrix $A = [\boldsymbol{a}_1, \boldsymbol{a}_2, \ldots, \boldsymbol{a}_n]$ of n subjects where row vector $\boldsymbol{a}_i = (a_{i1}, a_{i2}, \ldots, a_{im})$ is an m dimension presurgical connectome feature vector for subject i whose element values are the upper diagonal of the connectivity matrix D, and $\boldsymbol{y} = (y_1, y_2, \ldots, y_n)$ is an n-dimension vector of binary element values that represent the clinical outcome of each subject in the training data set (ie, the clinical outcome for row vector $\boldsymbol{a}_i$ is y_i). Because $m \gg n$, the elastic net (Zou and Hastie, 2005) sparse learning technique is used to find a sparse m dimension weight vector $\boldsymbol{x}$ that minimizes

$$\min_x \tfrac{1}{2}||\tilde{A}\boldsymbol{x} - \boldsymbol{y}||_2^2 + \lambda||\boldsymbol{x}||_1 + \tfrac{\rho}{2}||\boldsymbol{x}||_2^2,$$

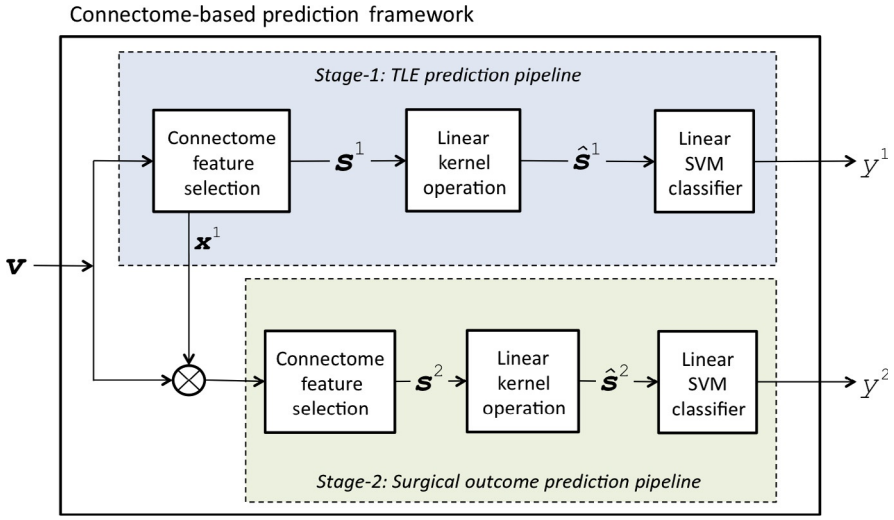

FIG. 16.2

Block diagram that illustrates the basic design and operation of the proposed connectome-based prediction framework. The framework defines two different prediction pipelines, specifically a Stage-1 prediction pipeline and a Stage-2 prediction pipeline. Each prediction pipeline has three trained components: (1) connectome feature selection, (2) linear kernel operation, and (3) linear SVM classifier. Note that the superscript value identifies the stage.

where $\lambda||\boldsymbol{x}||_1$ is the ℓ_1 regularization (sparsity) term, $\frac{\rho}{2}||\boldsymbol{x}||_2^2$ is the ℓ_2 regularization (smoothness) term, and $\tilde{A}$ is an $n \times m$ matrix with normalized training data. Specifically, $\tilde{A}\,(i,j) = (a_{ij} - a_{ij})/\sigma_j$, where a_{ij} is network connection j for subject i, a_{ij} is the mean value of column vector j in matrix A, and σ_j is the standard deviation of column vector j in matrix A. After optimization, $\boldsymbol{x}$ has weight values in [0 1], where weight values equal to zero indicate network connections that do not contribute to the clinical outcome, and weight values greater than zero indicate network connections that do contribute to the clinical outcome. In general, $\boldsymbol{x}$ is referred to as the sparse representation of the training data set. Lastly, each weight value in $\boldsymbol{x}$ greater than zero is set to one. Therefore the resulting sparse representation can be perceived as a binary mask, that is, the network connection is turned on (value of 1) or turned off (value of 0). A new sparse training data matrix is created, $S = [\boldsymbol{s_1}, \boldsymbol{s_2}, \ldots, \boldsymbol{s_n}]^t$, where row vector $\boldsymbol{s}_i = (a_{i1}x_1, a_{i2}x_2, \ldots, a_{im}x_m)$.

Even though the learned sparse representation can greatly reduce the dimension of the input connectome feature vector, the number of nonzero features in the newly created sparse training data matrix will most likely not be equal to the number of training data subjects. This condition may result in an overdetermined system of equations (with more subjects than features), or an underdetermined system of

equations (with more features than subjects). In both cases, there may be an infinite number of solutions, or no solution, to this system of linear equations, which in turn may severely impact the accuracy of the trained classifier. To overcome this limitation, a square $\tilde{m} \times \tilde{m}$ Gramian (Lanckriet, 2004) matrix $\hat{S} = S^t S$ is constructed, where S^t is the matrix transpose and $\tilde{m}$ is the number of nonzero features in the sparse representation. It is important to note that these more compact features cannot be mapped back to a single network connection. In fact, each feature in this newly formed mathematical space is the inner product of two network connection vectors.

Finally, $\hat{S}$ and $\boldsymbol{y}$ are used to train a linear two-class SVM classifier based on the LIBSVM library.[3] Once the SVM classifier is trained, the surgical treatment outcome of a high-dimension feature vector, say $\boldsymbol{v} = (v_1, \ldots, v_m)$, not in the training data set can be predicted using the following steps: (1) Normalize each value in $\boldsymbol{v}$ using the learned centering and magnitude scaling values for the $j = 1, \ldots, m$ network connection features $v_i = (v_i - a_{ij})/\sigma_j$. (2) Create sparse connectome feature vector $\mathbf{s} = (v_1 x_1, v_2 x_2, \ldots, v_m x_m)$ by applying learned binary weights. All features that have a zero value are removed, resulting in an $\tilde{m}$ dimension connectome feature vector. (3) Apply learned linear transformation to obtain $\tilde{m}$-dimension feature vector $\hat{\mathbf{s}} = \left(\hat{s}_1, \hat{s}_2, \ldots, \hat{s}_{\tilde{m}}\right)$, where $\hat{s}_i = \sum_{j=1}^{\tilde{m}} s_j \hat{S}(j, i)$ for $i = 1, \ldots, \tilde{m}$. (4) Calculate the predicted class label $y = \sum_{i=0}^{\tilde{m}} \alpha_i \kappa\left(\boldsymbol{\delta}_i, \hat{s}\right) + b$, where α are the weights, $\boldsymbol{\delta}$ are the support vectors, $\kappa(\cdot)$ is the inner product of the two vectors, and b is the bias that defines the linear hyperplane (decision boundary) learned by the SVM algorithm. The sign of the calculated prediction value (ie, $y \geq 0$ or $y < 0$) determines which of the two diagnosis labels the subject is assigned to.

16.2.5 RESULTS AND EVALUATION

The predictive power of the connectome-based framework is evaluated using a 10-fold cross-validation strategy. In particular, the Bonn and MUSC subjects are first combined into one data set, and then partitioned into 10 different folds, where each fold contains connectomes of randomly selected patients (ie, a mixture of seizure-free and not seizure-free) and/or randomly selected normal controls. The prediction framework is iteratively trained using the connectome data in nine of the 10 folds, and then tested using the connectome data in the remaining (or left-out) fold. This iterative process terminates when each fold has been selected as the test one. Using the combined confusion matrix (TP=true positive, FP=false positive, FN=false negative, and TN=true negative) results of each test fold, the prediction performance is reported using the specificity (SPE), sensitivity (SEN), positive predictive value (PPV), negative predictive value (NPV), and accuracy (ACC) measures.

[3] http://www.csie.ntu.edu.tw/$\sim$cjlin/libsvm/

16.2.5.1 Stage-1 TLE prediction pipeline

In this experiment, the total number of subjects in the connectome data set is 118, including 70 patients with TLE and 48 HCs. This data set was randomly partitioned into 10 folds, where 8 of the 10 folds have 12 subjects, and 2 of the 10 folds have 11 subjects. The number of subjects n in the training population is approximately 106, where each training subject is defined by $m = (81 \times 82)/2 = 3321$ dimension connectome feature vector. Lastly, the class labels used to train the prediction pipeline are 0=patient with TLE and 1=HC. The resulting performance of the TLE prediction pipeline was SEN=74%, SPE=88%, PPV=90%, NPV=70%, and ACC=80%. The total number of nonzero network connections $|w_t| = \cup_{f=1}^{10} w_f$ selected by the elastic net algorithm that can differentiate patients with TLE from HCs is 383, where w_t is the union of each learned sparse representation for each fold. Using a two-sample t-test with $\alpha = 0.05$ a paired p-value is calculated for each nonzero network connection in w_t and then sorted in ascending order, where the null hypothesis represents data that are independent random samples from normal distributions with equal means and equal but unknown variances. The top 15 nonzero network connections with the smallest p-values, that is, those with the greatest difference between the two groups, can be seen and visualized in Fig. 16.3.

16.2.5.2 Stage-2 surgical treatment outcome prediction pipeline

In this experiment, the total number of patients with TLE in this data set is 70 and it was also randomly partitioned into 10 folds, where each fold has 7 subjects. The

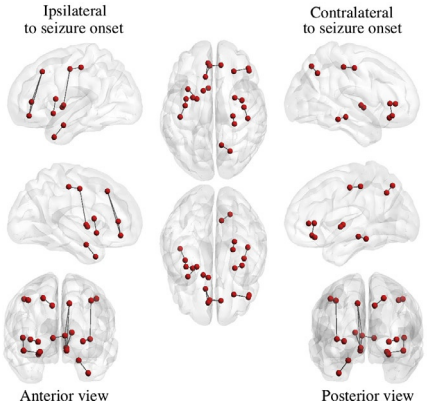

Region	-	Region
Ipsilateral insula	-	Ipsilateral putamen
Contralateral insula	-	Contralateral putamen
Ipsilateral precentral	-	Ipsilateral postcentral
Contralateral pars orbitalis	-	Contralateral parstriangularis
Ipsilateral superior frontal	-	Ipsilateral rostral anterior cingulate
Ipsilateral caudate	-	Ipsilateral accumbensarea
Contralateral precentral	-	Contralateral postcentral
Ipsilateral medial orbitofrontal	-	Ipsilateral superior frontal
Contralateral lateral orbitofrontal	-	Contralateral parsorbitalis
Contralateral rostral anterior cingulate	-	Ipsilateral rostral anterior cingulate
Ipsilateral precentral	-	Ipsilateral insula
Ipsilateral temporalpole		Ipsilateral amygdala
Ipsilateral medial orbitofrontal	-	Ipsilateral rostral anterior cingulate
Contralateral parahippocampal	-	Contralateral hippocampus
Contralateral superior parietal	-	Contralateral precuneus

FIG. 16.3

Stage-1 TLE results. The top 15 connected regions with the smallest p-value (ie, the network connections with the greatest difference between patients with TLE and HCs). The p-values are calculated using a two-sample t-test. The brain regions, defined using the Lausanne anatomical atlas, are represented by the red nodes (dark gray in print versions), and the edge connecting two brain regions represents a network connection in the connectome.

number of subjects n in the training population is 63, where each training subject is defined by an $m = 383$ dimension sparse connectome feature vector, found by the stage-1 connectome feature selection component. The class labels used to train the prediction pipeline are 0=not seizure-free and 1=seizure-free. The resulting performance of the TLE prediction pipeline was SEN=59%, SPE=76%, PPV=63%, NPV=74%, and ACC=70%. The total number of nonzero network connections $|w_t|$ selected by the elastic net algorithm (in the second stage of the proposed two-stage framework) that is able to differentiate the seizure-free postsurgery group from the not-seizure-free postsurgery group is 132. Using a two-sample t-test with $\alpha = 0.05$ a paired p-value is calculated for each nonzero network connection in w_t and then sorted in ascending order, where the null hypothesis represents data that are independent random samples from normal distributions with equal means and equal but unknown variances. The top 15 nonzero network connections with the smallest p-values, that is, those with the greatest difference between the two groups, can be seen and visualized in Fig. 16.4.

The results from this study also support the notion that epilepsy in general, and specifically TLE, are associated with temporal and extratemporal network architecture abnormalities (Bonilha, 2013; DeSalvo, 2013, 2014; Liu, 2014). They also indicate that a pattern of network abnormalities may be relevant on an individual basis to guide the estimation of clinical outcomes. While most studies to date have demonstrated the average effects on TLE on the structural connectome, the

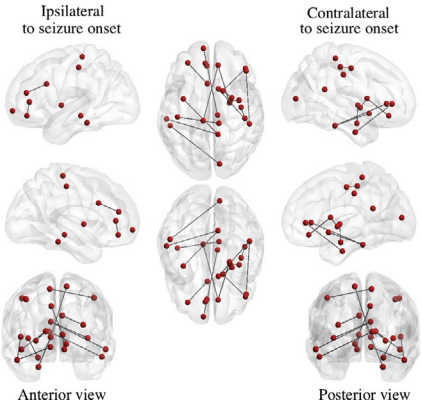

Region	-	Region
Contralateral posterior cingulate	-	Ipsilateral frontal pole
Contralateral paracentral	-	Ipsilateral postcentral
Contralateral insula	-	Contralateral amygdala
Contralateral inferior temporal	-	Contralateral accumbens area
Ipsilateral medial orbitofrontal	-	Ipsilateral rostra lanterior cingulate
Contralateral pericalcarine	-	Ipsilateral inferior temporal
Contralateral rostral anterior cingulate	-	Ipsilateral paracentral
Contralateral isthmus cingulate	-	Ipsilateral middle temporal
Contralateral parsorbitalis	-	Contralateral caudate
Contralateral pars triangularis	-	Contralateral inferior temporal
Contralateral rostral anterior cingulate	-	Contralateral entorhinal
Contralateral precentral	-	Contralateral postcentral
Contralateral caudate	-	Contralateral putamen
Ipsilateral rostral middle frontal		Ipsilateral caudal anterior cingulate
Contralateral isthmus cingulate	-	Ipsilateral insula

FIG. 16.4

Stage-1 TLE results. The top 15 connected regions with the smallest p-value (ie, the network connections with the greatest difference between the patients that are seizure-free after surgery and those that are not seizure-free after surgery). The p-values are calculated using a two-sample t-test. The brain regions, defined using the Lausanne anatomical atlas, are represented by the red nodes (dark gray in print versions), and the edge connecting two brain regions represents a network connection in the connectome.

application of machine learning to the connectome can disclose how the complexity of the connectome can be abridged to yield classifiers with clinical relevance. Importantly, the connectome is a rich and complex data set, and individuals with TLE may harbor abnormalities with inter-individual variability. Thus the use of machine learning can overcome some of these challenges, while incorporating the crucial parameters in the connectome that are relevant to epilepsy management. In this context, the connectome can be used not only to provide information about the neurobiology of the disease, but also to provide information about the personalized clinical trajectory. This trajectory cannot be accurately defined based on the existing clinical measures, and machine learning applied to the connectome may unveil a completely new avenue for additional clinical phenotyping and management planning. One very interesting observation is that the connectome-based prediction framework can achieve roughly the same accuracy as expert clinical opinion. Historically speaking, presurgical diagnostics using expert-based clinical information are approximately 70% accurate for patients that choose to have surgery. In this study, the prediction framework is also 70% accuracy. This level of accuracy is achieved based on the connectome alone, which is pretty remarkable, and is an important clinical finding that may advance outcome prediction for patients with epilepsy.

16.3 NAMING IMPAIRMENT PERFORMANCE OF PATIENTS WITH TLE

16.3.1 PARTICIPANTS

We retrospectively studied a group of 24 patients with medication refractory TLE. All patients had language dominance mapped to the left hemisphere through the WADA test. All patients had medically refractory TLE, diagnosed according to the criteria defined by the International League Against Epilepsy (ILAE, 1989), including a comprehensive neurological evaluation, electroencephalography (EEG) recordings, diagnostic MRI, and, when appropriate, nuclear medicine studies.

16.3.2 LANGUAGE ASSESSMENT

Table 16.1 outlines the language tests used in this study. Specifically, testing included six subtests from the 1983 edition of Boston Diagnostic Aphasia Examination (BDAE) that were designed to be understood by all patients, at all reading levels. For convenience the descriptions provided below are from the Assessment of Aphasia and Related Disorders (Goodglass et al., 2000). Even though the purpose of this study was to evaluate naming performance, measures of repetition and comprehension were included to provide a more comprehensive evaluation of language performance and to elucidate whether individual naming impairments were isolated deficits or part of global language impairments. All the test scores were normalized to a value in

Table 16.1 Name and Description of Each Test Used in the Aphasia Language Assessment

Test	Description
Basic word discrimination (BWD)	Stimulus items included five body parts and 31 picture cards (color, letter, or number). For body parts, patients were instructed to point to the corresponding location. For picture cards, patients were instructed to point to the picture corresponding to the spoken test word. Patients received 1 point per item if the response was correct within 5 s and 1/2 point if the response was correct in more than 5 s. Responses were scored out of 37. The choice of items samples many different categories, targeting categories that are frequently affected or unaffected in aphasic patients.
Verbal agility (VBA)	Patients repeated seven groups of test words as rapidly as possible and the number of repetitions completed within 5 s was recorded. Results were recorded out of a total possible score of 14. Performance on the verbal agility test is correlated with aphasic articulation difficulties and does not rely explicitly on memory or word retrieval, it just requires patients to produce continuous speech.
Repetition (REP)	Patients were instructed to repeat single words back to the examiner. Credit was only given if the word was intelligible, but records were made for articulation impairment. Results were scored out of a possible 10.
Boston naming test (BNT)	The BNT was administered using the Standard form of 60 picture items. Correct responses, latency in seconds, items requiring stimulus cues, and items requiring phonemic cues were recorded. Responses that were erroneous were also recorded. Items that could be answered correctly with the addition of multiple-choice options were also recorded. Credit was allowed for correct oral naming only.
Picture word matching (PWM)	Ten pictures were used for word identification examination. The examiner pointed to each picture and asked the patient to find its name among four word choices offered. Answer choices include the correct answer along with semantic and structural distracters of varying difficulty.
Sentence paragraph comprehension (SPC)	Patients were shown a primary sample sentence and four choices to complete it. Patients were given the option to have the examiner read the sentence and each of the choices aloud and select the correct completion. Patients were then instructed to read the 10 test sentences to him or her and point to the correct completion. Results were recorded out of a possible score of 10.

[0 1], where 0 indicates the patient did not correctly answer any test questions, and 1 indicates the patient correctly answered all the test questions correctly.

16.3.3 IMAGE ACQUISITION AND PROCESSING

The same imaging protocol was applied to all study participants. All subjects were scanned in a Siemens 3T Verio MRI scanner equipped with a 12-channel head

coil. The imaging protocol yielded a high-resolution T1-weighted image with an isometric voxel size of 1 mm. Diffusion-weighted images were obtained using a twice-refocused echo planar sequence with three diffusion weightings. DICOM images were converted to NIfTI format using the MRIcron software toolbox. The FMRIB software library diffusion toolkit (FDT) was used for preprocessing diffusion-weighted images and also for diffusion tensor estimation. The images underwent eddy current correction through affine transformation of each DWI to the base $b = 0$, T2-weighted image.

16.3.4 CONNECTOME RECONSTRUCTION

Probabilistic tractography was used to define the number of white matter streamlines connecting each pair of cortical regions, which were defined according to the Lausanne anatomical atlas. This step was performed iteratively until the connectivity between all possible pairs of cortical regions was determined. The connectivity information was then compiled in an individual brain connectome (ie, symmetric two-dimensional connectivity matrix). Specifically, cortical seed regions for tractography were obtained through an automatic segmentation process employing FreeSurfer on the T1-weighted images, dividing the human cerebral cortex into cortical and subcortical ROIs, automatically assigning a neuroanatomical label to each location on a cortical surface model yielding 82 ROIs in the subjects' native T1-weighted space (41 regions in each hemisphere). All processed images were visually inspected to ensure the cortical segmentation quality. The ROIs were transformed into each subject's DTI space using an affine transformation obtained with FSL's FLIRT. Probabilistic tractography was performed using each of the 82 cortical ROIs in diffusion space as the seed region.

For each subject, a comprehensive neuronal connectivity map, or connectome, was calculated where the connectivity is measured by the number of probabilistic white matter fiber tract streamlines arriving at ROI j when ROI i was seeded, averaged with the number of probabilistic white matter fiber tract streamlines arriving at ROI i when ROI j was seeded. This step is iteratively repeated to ensure all 82 cortical ROIs are treated as seed regions, resulting in a symmetric 82×82 density connectivity map D, where D_{ij} is the weighted network connection between ROIs i and j. Since the numbers of streamlines are averaged between each ROI, D is symmetric with respect to the main diagonal. Example connectomes are shown in Fig. 16.5 that is created using the described reconstruction procedure.

16.3.5 CONNECTOME PREDICTION FRAMEWORK

Fig. 16.6 illustrates the basic design and operation of the proposed language prediction framework. In particular, the framework includes a connectome feature selection component that uses a multitask machine learning algorithm followed by a prediction component that consists of a bank of support vector regression (SVR) prediction models, one for each language assessment task used in this study. It is

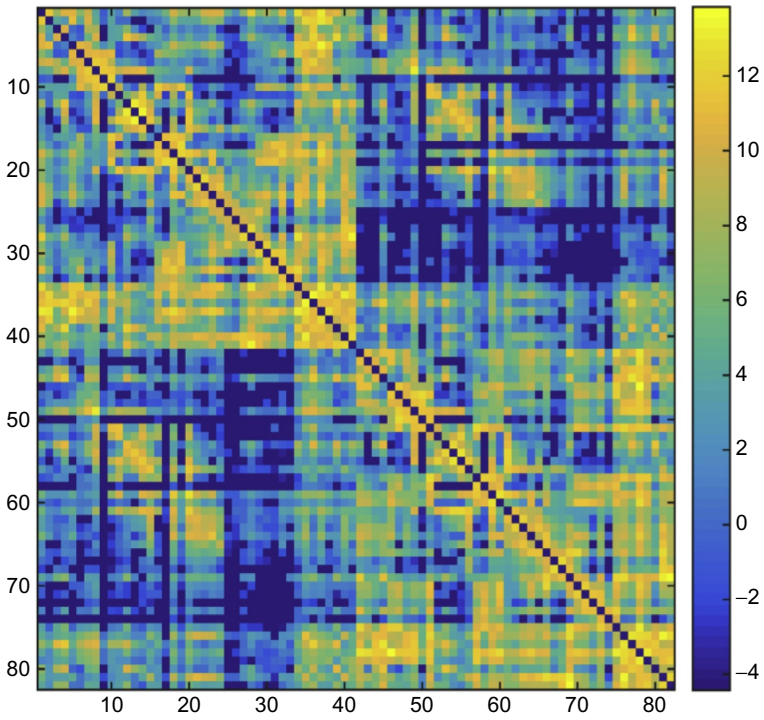

FIG. 16.5

Example of a symmetric 82 × 82 connectivity map for one representative subject. The brain structures are numbered from 1 to 82 in accordance with the atlas. The values in the scale bar illustrate logarithm of link strength.

important to note that each component in the prediction framework is trained with connectome features that are calculated using only one graph-theoretic measure (v). Therefore for the prediction framework to work correctly the graph-theoretic measure used to calculate the input connectome features represented by a^{υ} must be the same graph-theoretic measure used to train the entire framework. The multitask feature selection is used to choose nodes whose graph-theoretic measures are jointly predictive of all language tasks. Given that TLE is typically associated with poor performance on the BNT that is out of proportion to other language impairment, most of the variance in the multitask feature selection comes from the BNT. Nonetheless, by performing the multitask feature selection including all language tests, we ensured that nodes associated with language performance other than naming were also chosen for the subsequent steps, which then directly tests the subnetwork in relationship with the BNT. For this reason, the multitask feature selection controls for the influence of the other language measures (besides naming) on the subnetwork that is subsequently

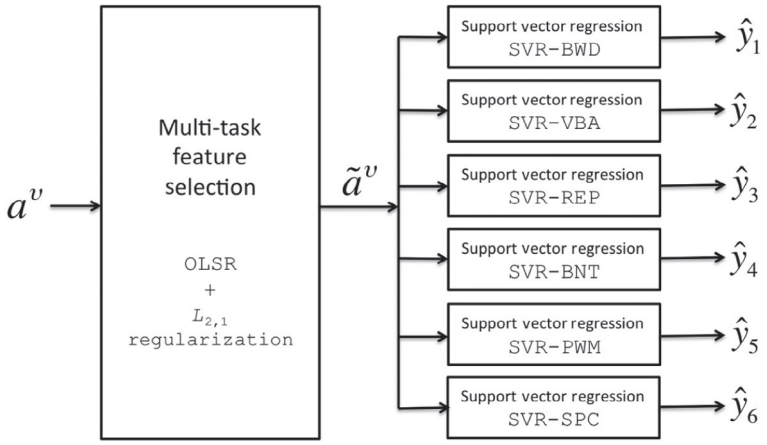

FIG. 16.6

Proposed language prediction framework that includes two trained components that are sequentially applied to connectome features *a* (found using graph-theoretic measure *v*) that is able to predict the test scores for the six language tasks: multitask feature selection using basic word discrimination (BWD), verbal agility (VBA), repetition (REP), Boston naming test (BNT), picture word matching (PWM), and sentence paragraph comprehension (SPC).

tested as predictive of BNT scores. Lastly, the output of the multitask feature selection component is input into a bank of six independent prediction models (one for each language task) that are able to predict the basic word discrimination (BWD), verbal agility (VBA), repetition (REP), Boston naming test (BNT), picture word matching (PWM), and sentence paragraph comprehension (SPC) language scores.

For each subject we created an $m = 82$ dimension connectome feature vector $\boldsymbol{a}^v = (a_1^v, \ldots, a_i^v, \ldots, a_m^v)$ using the connectivity values in D as the eigenvector centrality graph-theoretic measure (Rubinov and Sporns, 2010) (denoted by v). In general, the selected graph-theoretic measure allows us to quantify how a brain region influences the network. Specifically, this measure quantifies regional connectivity by identifying highly connected brain regions, which are connected to neighboring brain regions that are also highly connected. The eigenvector centrality measure for ROI i is $a_i = |\lambda_i|$, where $|\lambda_i|$ is the absolute value of the ith eigenvalue. More specifically, the m eigenvalues $(\lambda_1, \lambda_2, \ldots, \lambda_m)$ are found by performing the eigen decomposition on D.

Given a normalized $n \times m$ training data matrix $A^v = \left[\boldsymbol{a}_1^v, \boldsymbol{a}_2^v, \ldots, \boldsymbol{a}_n^v\right]$ of n subjects where row vector $\boldsymbol{a}_i^v$ is the connectome feature vector for subject i found using graph measure v, and an $n \times k$ training label matrix $Y = \left[\boldsymbol{y}_1, \boldsymbol{y}_2, \ldots, \boldsymbol{y}_n\right]$ where the elements in row vector $\boldsymbol{y}_i = (y_{i1}, y_{i2}, \ldots, y_{ik})$ represent the known $k = 6$ language test scores for subject i (y_{i1} is the BWD test score, y_{i2} is the VBA test score, etc.), an ordinary least squares linear regression (OLSR) algorithm, which includes an $\ell_{2,1}$

regularization term (Gong, 2013), is used to find a sparse $m \times k$ dimension weight matrix X^{υ} that minimizes

$$\min_{x} \tfrac{1}{2}||A^{\upsilon}X^{\upsilon} - Y||_2^2 + \lambda||X^{\upsilon}||_{2,1},$$

where $\lambda||X^{\upsilon}||_{2,1}$ is the regularization term. The above equation is optimized using the *mcLeastR* function in the Sparse Learning with Efficient Projections software package.[4] After optimization, X^{υ} has weight values in [0 1] where values greater than zero indicate brain regions that contribute to the language tasks. The weight matrix X^{υ} is then used to find an m dimension vector:

$$\boldsymbol{x^{\upsilon}} = \left(\sqrt{\sum_{j=1}^{k}(X_{1j}^{\upsilon}X_{1j}^{\upsilon},)}, \ldots, \sqrt{\sum_{j=1}^{k}(X_{mj}^{\upsilon}X_{mj}^{\upsilon})}\right),$$

that is commonly referred to as the sparse representation of the training data set. In our approach weight values greater than zero are set to 1, therefore the resulting sparse representation becomes a binary mask. That is, a brain region is turned on (value of 1) or turned off (value of 0). A new $n \times m$ sparse training data matrix is created $\tilde{A}^{\upsilon} = \left[\tilde{\boldsymbol{a}}_1^{\upsilon}, \tilde{\boldsymbol{a}}_2^{\upsilon}, \ldots, \tilde{\boldsymbol{a}}_n^{\upsilon}\right]$, where row vector $\tilde{\boldsymbol{a}}_i^{\upsilon} = \left(a_{i1}^{\upsilon}x_1^{\upsilon}, a_{i2}^{\upsilon}x_2^{\upsilon}, \ldots, a_{im}^{\upsilon}x_m^{\upsilon}\right)$.

The sparse connectome feature matrix $\tilde{A}^{\upsilon}$ and the known language test score matrix Y are then used to train a bank of support vector regression (SVR) prediction models, specifically one prediction model for each language task as shown in Fig. 16.2. In particular, a linear ε-SVR prediction model (Vapnik, 1998), which is based on the LIBSVM library (Chang and Lin, 2011), is independently trained for each language task. Once each ε-SVR prediction model is trained, the six language scores can be predicted using the three steps: (1) Calculate the normalized $\boldsymbol{a}^{\upsilon}$, the connectome feature vector using graph measure υ; (2) create sparse feature vector $\tilde{\boldsymbol{a}}^{\upsilon}$ by applying learned binary weights in x^{υ} to $\boldsymbol{a}^{\upsilon}$; and (3) calculate the predicted language score $\hat{y}_k = \sum_{i=1}^{m}\left(\alpha_i - \alpha_i^*\right)\langle\boldsymbol{\phi}_i, \tilde{\boldsymbol{a}}^{\upsilon}\rangle + b$ for tasks $k = 1$–6, where $\langle\cdot\rangle$ is the inner product of two vectors, $\alpha_i^{(*)}$ is the regression weight, ϕ_i is the support vector, and b is the bias that defines the linear regression line learned by the ε-SVR algorithm.

16.3.6 RESULTS AND EVALUATION

For each graph-theoretic measure (υ) a prediction framework is constructed and the performance is assessed using a leave-one-out cross-validation (LOOCV) strategy that iteratively removes one subject from the population as the test subject, and the remaining subjects are used to train the prediction framework. For each leave-one-out test subject $l = 1, 2, \ldots, n$, the predicted language scores $\hat{\boldsymbol{y}}_l = \left(\hat{y}_{l1}, \hat{y}_{l2}, \ldots, \hat{y}_{lk}\right)$ are calculated. Finally, the mean square error $\text{MSE}_k = \frac{1}{n}\sum_{l=1}^{n}\left|y_{lk} - \hat{y}_{lk}\right|$ for the $k = 1, 2, \ldots, 6$ language tests are calculated where $\boldsymbol{y}_l = (y_{l1}, y_{l2}, \ldots, y_{lk})$ is the

[4] *http://www.public.asu.edu/~jye02/Software/SLEP*

Table 16.2 Prediction Framework Results for the Six Language Tests, and for the Eigenvector Graph-Theoretic Measure

	Eigenvector Centrality	
Language Tests	**MSE**	R^2
Basic word discrimination (BWD)	0.002	0.99
Verbal agility (VBA)	0.010	0.44
Repetition (REP)	0.008	0.99
Boston naming test (BNT)	0.035	0.60
Picture word matching (PWM)	0.013	0.72
Sent paragraph comprehension (SPC)	0.041	0.75

The average regression correlation coefficient (R^2) measures how well the linear regression line found by the ε-SVR algorithm fits the connectome features to the known language scores.

known language scores for test k, and $|\cdot|$ is the absolute value. If the MSE value is zero then the predicted language test score is identical to the known language test score.

The language prediction results are summarized in Table 16.2, trained and tested using connectome features found using the eigenvector graph-theoretic measure. Additionally, Table 16.2 includes the average regression correlation coefficient (R^2) value, which discloses the linear regression found by the e-SVR algorithm in relationship with the language scores, that is, how well the predicted scores correlated with the known scores. Given that in the LOOCV training procedure $n = 24$ prediction frameworks are created, 24 prediction models are created for each of the six language tests, therefore the reported R^2 language test k is $\frac{1}{n}\sum_{i=1}^{n} R_k^2$.

The results in Fig. 16.7 and Table 16.3 show the brain regions that have the greatest frequency in the learned binary sparse representation found by the multitask feature selection component when connectome features are calculated using the eigenvector centrality graph-theoretic measure. The results in Table 16.3 also show the average ROI regression weight calculated using each of the $k = 6\varepsilon$-SVR regression models in each of the $n = 24$ prediction frameworks. Specifically, the average regression weight for ROI i is $\bar{r}_i^{\upsilon} = \frac{1}{nk}\sum_{j\in n, t\in k} r_{tj}^{\upsilon}$ where r_{tj}^{υ} is the ε-SVR regression weight for prediction framework j and language task t when graph measure υ is used. In general, an average regression weight that makes a value of zero indicates the brain region does not contribute to any of the language tasks and a very large average regression weight indicates the brain region has a significant contribution to one or more of the language tasks. In summary, if a brain region in Table 16.3 has a large frequency value and a large average regression weight value, then this brain region makes a significant contribution to one or more of the language tasks.

From nodal regression weights within the eigenvector centrality model, it is possible to observe that this subnetwork is strongly dependent on medial temporal structures, including the entorhinal cortex and basal nuclei (pallidum and putamen),

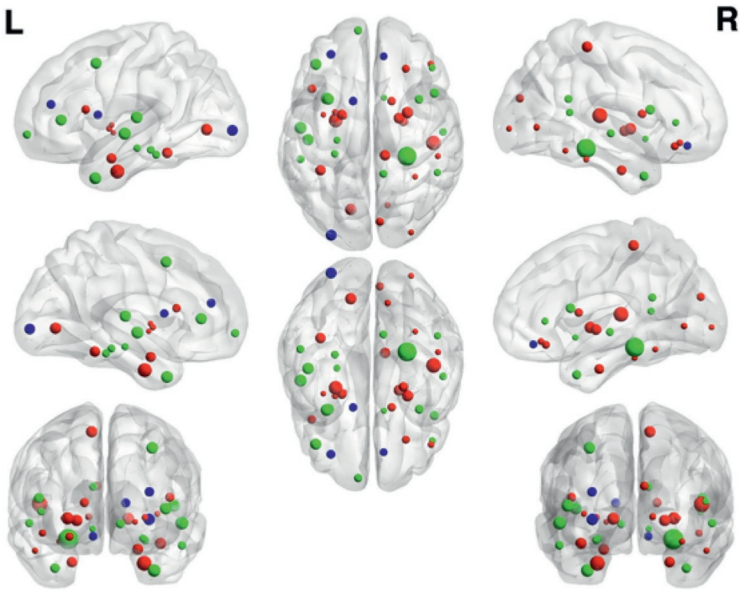

FIG. 16.7

Brain regions that have the greatest frequency among the $n = 25$ binary sparse representations found by the multitask feature selection component and connectome features calculated using the eigenvector graph-theoretic measure. Node color is based on frequency in sparse representation (gray = 100%, light gray 99–90%, dark gray 89–80%). These features are described in detail in the accompanying Table 16.3. Furthermore, the size of the node is related to the average regression weight shown in Table 16.3.

Table 16.3 Accompanying Legend to Fig. 16.7

Rank	Frequency in Sparse Representation	Average Regression Weight (Across the Six SVR Models)	Node Color in Visualization	Region Description
1	100%	4.12	Red	Right transverse temporal
2	100%	3.81	Red	Left entorhinal
3	100%	2.83	Red	Right putamen
4	100%	2.81	Red	Left lingual
5	100%	2.57	Red	Right pallidum
6	100%	2.48	Red	Right paracentral
7	100%	2.46	Red	Left fusiform
8	100%	2.30	Red	Left amygdala
9	100%	2.14	Red	Right entorhinal

Continued

Table 16.3 Accompanying Legend to Fig. 16.7—cont'd

Rank	Frequency in Sparse Representation	Average Regression Weight (Across the Six SVR Models)	Node Color in Visualization	Region Description
10	100%	1.69	Red	Right caudate
11	100%	1.67	Red	Left parsopercularis
12	100%	1.54	Red	Right cuneus
13	100%	1.47	Red	Right lateral orbitofrontal
14	100%	0.98	Red	Right parsorbitalis
15	100%	0.89	Red	Right lingual
16	100%	0.85	Red	Left putamen
17	100%	0.66	Red	Right inferior temporal
18	100%	0.65	Red	Right lateral occipital
19	100%	0.64	Red	Right fusiform
20	100%	0.55	Red	Left insula
21	100%	0.46	Red	Left pallidum
22	96%	5.76	Green	Right parahippocampal
23	96%	2.96	Green	Left temporal pole
24	96%	2.62	Green	Left caudal middle frontal
25	96%	2.00	Green	Right parsopercularis
26	96%	1.45	Green	Left inferior temporal
27	96%	1.41	Green	Right isthmuscingulate
28	96%	1.37	Green	Left parahippocampal
29	96%	1.12	Green	Right bankssts
30	96%	1.11	Green	Left hippocampus
31	96%	1.05	Green	Right parstriangularis
32	96%	0.72	Green	Right accumbens area
33	92%	3.10	Green	Left superior temporal
34	92%	2.85	Green	Left transverse temporal
35	92%	2.66	Green	Left parstriangularis
36	92%	1.84	Green	Right temporal pole
37	92%	1.55	Green	Left frontal pole
38	92%	1.39	Green	Right superior temporal

Continued

Table 16.3 Accompanying Legend to Fig. 16.7—cont'd

Rank	Frequency in Sparse Representation	Average Regression Weight (Across the Six SVR Models)	Node Color in Visualization	Region Description
39	88%	1.84	Blue	Left rostral middle frontal
40	88%	1.74	Blue	Left caudate
41	83%	2.57	Blue	Left lateraloccipital
42	83%	1.44	Blue	Right medial orbitofrontal

Within the multitask feature selection, the largest frequency in sparse representation is 100%, and the smallest frequency is 0. A frequency of 100% indicates that this brain region was selected by the group LASSO algorithm in all 24 LOOCV folds, and a frequency of 0% means the group LASSO algorithm, in any LOOCV fold, did not select the brain region. Within all six ε-SVR regression models and all 24 LOOCV folds an average regression weight that has a value of zero indicates that this brain region does not contribute to any of the language tasks and a very large average regression weight indicates that this brain region makes a significant contribution to one or more of the language tasks.

followed by other medial temporal structures (eg, parahippocampal gyri, hippocampi and amydgala) and frontal regions. Given the high frequency of memory problems in subjects with difficult to control TLE (Elger, 2004), these results may indicate that naming performance in TLE is mostly associated with the structures supporting memory function, notably the circuitry involving the connections between *medial temporal to lateral temporal to basal nuclei to frontal regions.* As such, among all necessary components involved in naming may disproportionately emphasize the semantic integration and symbol retrieval processes, as opposed to multimodal recognition and speech production.

Naming impairments in TLE are associated with the structural preservation of a subnetwork, which includes gray matter regions located mostly in the temporal and frontal areas. Approximately 60% of naming performance on the BNT can be predicted by a measure of integration of the nodes in this subnetwork termed eigenvector centrality. These results confirm the assumption that language and, more specifically, naming, which are higher cognitive functions, rely on the concerted action among multiple regions, as opposed to being dependent on isolated brain areas. Nonetheless, the generalization of these results to other neurological conditions associated with naming impairment, or to normal brain function, should take into account that the disproportionate participation of right hemisphere nodes in the predictive model may be related to chronic and gradual network rearrangements in epilepsy and the chronic compensatory role of the right hemisphere. Furthermore, this distributed network may also be unequally influenced by memory problems associated with TLE, being more sensitive to memory-dependent aspects of naming such as semantic integration and communicative symbol retrieval, as opposed to multimodal perception or speech production.

REFERENCES

Babb, T.L., Brown, W.J., 1987. Pathological Findings in Epilepsy. Raven Press, New York, pp. 511–540 .

Bartzokis, G., 2004. Age-related myelin breakdown: a developmental model of cognitive decline and Alzheimer's disease. Neurobiol. Aging 25 (1), 5–18.

Behrens, T., 2003. Characterization and propagation of uncertainty in diffusion-weighted MR imaging. Magn. Reson. Med. 50 (5), 1077–1088.

Behrens, T., 2007. Probabilistic diffusion tractography with multiple fibre orientations: what can we gain? NeuroImage 34 (1), 144–155.

Berg, A.T., 2010. Revised terminology and concepts for organization of seizures and epilepsies: report of the ILAE commission on classification and terminology, 2005–2009. Epilepsia 51 (4), 676–685.

Bernasconi, N., 2003. Mesial temporal damage in temporal lobe epilepsy: a volumetric MRI study of the hippocampus, amygdala and parahippocampal region. Brain 126 (Pt 2), 462–469.

Bernasconi, N., 2004. Whole-brain voxel-based statistical analysis of gray matter and white matter in temporal lobe epilepsy. NeuroImage 23 (2), 717–723.

Bernhardt, B.C., 2008. Mapping limbic network organization in temporal lobe epilepsy using morphometric correlations: insights on the relation between mesiotemporal connectivity and cortical atrophy. NeuroImage 42 (2), 515–524.

Besson, P., 2014. Structural connectivity differences in left and right temporal lobe epilepsy. NeuroImage 100, 135–144.

Bonilha, L., 2003. Medial temporal lobe atrophy in patients with refractory temporal lobe epilepsy. J. Neurol. Neurosurg. Psychiat. 74 (12), 1627–1630.

Bonilha, L., 2004. Voxel-based morphometry reveals gray matter network atrophy in refractory medial temporal lobe epilepsy. Arch. Neurol. 61 (9), 1379–1384.

Bonilha, L., 2012. Subtypes of medial temporal lobe epilepsy: influence on temporal lobectomy outcomes? Epilepsia 53 (1), 1–6.

Bonilha, L., 2013. Presurgical connectome and postsurgical seizure control in temporal lobe epilepsy. Neurology 81 (19), 1704–1710.

Bonilha, L., 2015. The brain connectome as a personalized biomarker of seizure outcomes after temporal lobectomy. Neurology 84 (18), 1846–1853.

Chang, C.C., Lin, C.J., 2011. LIBSVM: a library for support vector machines. ACM Trans. Interact. Intell. Syst. 2 (3), 1–27.

Ciccarelli, O., 2006. Probabilistic diffusion tractography: a potential tool to assess the rate of disease progression in amyotrophic lateral sclerosis. Brain 129 (7), 1859–1871.

Crossley, N.A., 2014. The hubs of the human connectome are generally implicated in the anatomy of brain disorders. Brain 137 (Pt 8), 2382–2395.

Daianu, M., 2013. Breakdown of brain connectivity between normal aging and alzheimer's disease: a structural k-core network analysis. Brain Connect. 3 (4), 407–422.

DeSalvo, M.N., 2013. Altered structural connectome in temporal lobe epilepsy. Radiology 270 (3), 842–848.

DeSalvo, M.N., 2014. Altered structural connectome in temporal lobe epilepsy. Radiology 270 (3), 842–848.

Elger, C.E., 2004. Chronic epilepsy and cognition. Lancet Neurol. 3 (11), 663–672.

Engel, J., 2003. Practice parameter: temporal lobe and localized neocortical resections for epilepsy report of the quality standards subcommittee of the American Academy

of Neurology, in association with the American Epilepsy Society and the American Association of Neurological Surgeons. Neurology 60 (4), 538–547.
Focke, N.K., 2008. Voxel-based diffusion tensor imaging in patients with mesial temporal lobe epilepsy and hippocampal sclerosis. NeuroImage 40 (2), 728–737.
Gong, P., 2013. Multi-stage multi-task feature learning. Adv. Neural Inform. Process. Syst. 14, 2979–3010.
Goodglass, H., et al., 2000. The Assessment of Aphasia and Related Disorders, third ed. Lippincott Williams & Wilkins, Philadelphia.
Hagmann, P., et al., 2008. Mapping the structural core of human cerebral cortex. PLoS Biol. 6 (7), e159.
Heiervang, E., 2006. Between session reproducibility and between subject variability of diffusion MR and tractography measures. NeuroImage 33 (3), 867–877.
ILAE, 1989. Proposal for revised classification of epilepsies and epileptic syndromes. Epilepsia 30 (4), 389–399.
Keller, S.S., Roberts, N., 2008. Voxel-based morphometry of temporal lobe epilepsy: an introduction and review of the literature. Epilepsia 49 (5), 741–757.
Lanckriet, G.R., 2004. Learning the kernel matrix with semidefinite programming. J. Mach. Learn. Res. 5, 27–72.
Liu, M., 2014. Disrupted anatomic white matter network in left mesial temporal lobe epilepsy. Epilepsia 55 (5), 674–682.
Nucifora, P.G., 2007. Diffusion-tensor MR imaging and tractography: exploring brain microstructure and connectivity 1. Radiology 245 (2), 367–384.
Richardson, M.P., 2012. Large scale brain models of epilepsy: dynamics meets connectomics. J. Neurol. Neurosurg. Psychiat. 83 (12), 1238–1248.
Rubinov, M., Sporns, O., 2010. Complex network measures of brain connectivity: uses and interpretations. NeuroImage 52 (3), 1059–1069.
Rubinov, M., Bullmore, E., 2013. Schizophrenia and abnormal brain network hubs. Dial. Clin. Neurosc. 15 (3), 339–349.
Spencer, S.S., 2002. Neural networks in human epilepsy: evidence of and implications for treatment. Epilepsia 43 (3), 219–227.
Sporns, O., 2011. The human connectome: a complex network. Ann. NY Acad. Sci. 1224, 109–125.
Sporns, O., 2013. The human connectome: origins and challenges. NeuroImage 80, 53–61.
Sporns, O., et al., 2005. The human connectome: a structural description of the human brain. PLoS Comput. Biol. 1 (4), e42.
Vapnik, V.N., 1998. Statistical Learning Theory. Wiley, New York.
Xie, T., He, Y., 2011. Mapping the Alzheimer's brain with connectomics. Front. Psychiat. 2, 77.
Zou, H., Hastie, T., 2005. Regularization and variable selection via the elastic net. J. R. Stat. Soc. B 67 (2), 301–320.